Electronic Supplementary Material (ESI) for Journal of Materials Chemistry C.

Electronic Supplementary Information

Highly Efficient Thermally Activated Delayed Fluorescence Emitters Enabled by Double Charge Transfer Pathways *via* Ortho-Linked Triarylboron/Carbazole Hybrids

Minting Ouyang,[a] Longjiang Xing,[a] Qiaodeng Chen,[a] Hong Huang,[b] Minrong Zhu,[b] Kai Hu,[a] Yuan Liu,[a] Wen-Cheng Chen,*[a] Yanping Huo[a] and Chuluo Yang*[b]*

[a] School of Chemical Engineering and Light Industry, Guangdong University of Technology, Guangzhou 510006, China. E-mail: liuyuancc@gdut.edu.cn (Y. Liu); wencchen@gdut.edu.cn (W-C. Chen).

[b] College of Materials Science and Engineering, Shenzhen University, Shenzhen 518060, China. E-mail: clyang@szu.edu.cn (C. Yang).

General information

All reagents were commercially available and used without further purification unless otherwise noted. ^1H NMR and ^{13}C NMR spectra were recorded on a Bruker AVANCE III HD 400 spectrometer using tetramethyl silane (TMS) as the internal standard. MALDI-TOF mass spectra were performed on a Bruker autoflex speed mass spectrometer, while ESI-TOF mass spectra were recorded on an Agilent 6210 ESI-TOF spectrometer. UV-visible absorption spectra were obtained on a Shimadzu UV-2700 spectrophotometer. Steady-state photoluminescence (PL) spectra were reported by a HORIBA Fluoromax-4C-L spectrophotometer, while time resolved PL spectra and transient PL spectra were detected on an Edinburgh Analytical instrument FLS980. Absolute PLQYs of all samples were measured on an Edinburgh Analytical instrument FLS980 equipped with an Edinburgh SM4 Integrating Sphere and all samples were excited at 340 nm, using a blank quartz plate as reference. Thermogravimetric Analysis (TGA) was performed on a NETZSCH STA409PC unit at a heating rate of 10 °C/min from 25 to 700 °C under N_2. Differential scanning calorimetry (DSC) were carried out on METTLER TOLEDO DSC3 at a heating rate of 10 °C/min from -60 to 300 °C for *o*B-2Cz and from -60 to 350 °C for *o*B-2*t*Cz under N_2. The glass transition temperature (T_g) was determined from the second heating scan at a heating rate of 10 °C/min. Cyclic voltammograms (CVs) were recorded on a CHI voltammetric analyzer, using tetrabutylammonium hexafluorophosphate ($TBAPF_6$) (0.1M) dissolved in dichloromethane (DCM) as the supporting electrolyte. The conventional three-electrode configuration consists of a platinum column working electrode, a platinum wire auxiliary electrode, and an Ag wire pseudo reference electrode with ferrocene (Fc/Fc^+) as the internal standard. The HOMO energy levels (eV) of the compounds were calculated according to the formula: $-[4.8+(E_{onset}-E_{1/2}(Fc/Fc^+))]$ eV.

Computational methods

Theoretical simulations were performed using the Gaussian 09 program packages. The density functional theory (DFT) calculations at the B3LYP(D3)/def2-SVP level were used to optimize the ground state geometries of the investigated molecules. Time-dependent density functional theory (TD-DFT) calculations were performed at PBE0/def2-SVP using the optimized ground state geometries. The hole/particle overlaps were deduced from the natural transition orbitals (NTOs) analysis based on TD-DFT results. Utilizing the overlap integral function embedded in Multiwfn, the overlap integrals between the highest occupied NTO (HONTO) and the lowest unoccupied NTO (LUNTO) could be calculated.

Device fabrication and characterization

Devices were prepared on indium tin oxide (ITO) coated glass substrates with a sheet resistance of 15 Ω/sqrt. Before use, the substrates were swabbed with Decon-90 solution, and treated by 15-min ultrasonic baths in deionized water before rinsing with isopropanol. The substrates were dried with N_2 flow to remove the residual solvent, and then were stored in an oven at 120 °C for at least 2 h. After UV-ozone treatment (15 min), the substrates were loaded into a deposition chamber with vacuum better than 10^{-6} Torr. Current density-voltage characteristics and electroluminescence spectrum were recorded with a Keithley 2400 power source and a PMA-12 photonic multichannel analyzer (Hamamatsu), respectively. Device measurement was performed under ambient conditions without encapsulation.

Synthesis of materials

9,9’-(2-bromo-1,3-phenylene)bis(9H-carbazole) (Compound 1), 9,9’-(2-bromo-1,3-phenylene)bis(3,6-di-tert-butyl-9H-carbazole) (Compound 2), 9,9’-(2-(dimesitylboranyl)-1,3-phenylene)bis(9H-carbazole) (*o*B-2Cz) and 9,9’-(2-(dimesitylboranyl)-1,3-phenylene)bis(3,6-di-tert-butyl-9H-carbozole) (*o*B-2*t*Cz) were synthesized according to the literature methods.[1-3]

Synthesis of *o*B-2Cz

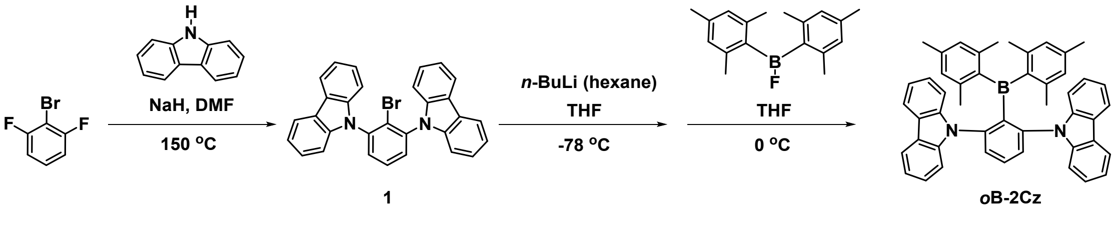

Scheme S1 Synthetic route of *o*B-2Cz.

Under Ar atmosphere, 9*H*-carbazole (57 mmol, 9.5 g) and NaH (114 mmol, 2.7 g) were mixed in anhydrous DMF (108 mL). After stirring at room temperature for 2 hours, 2-bromo-1,3-difluorobenzene (25.9 mmol, 5 g) was added and then refluxed overnight. After cooling to room temperature, the mixture was poured into water and extracted with CH_2Cl_2 by three times. The combined organic layer was washed with water and dried over Na_2SO_4. The solvent was removed under reduced pressure and the crude product was purified by silica gel column chromatography using *n*-hexane/CH_2Cl_2 (4:1, *v*/*v*) as eluent and compound 1 was obtained as white powder. Yield: 50% (12.9 mmol, 6.3 g). ^{1}H NMR (400 MHz, $CDCl_3$) δ (ppm) 8.17 (d, J = 7.7 Hz, 4H), 7.76 (dd, J = 9.1, 6.2 Hz, 1H), 7.73 – 7.68 (m, 2H), 7.50 – 7.45 (m, 4H), 7.35 – 7.31 (m, 4H), 7.21 (d, J = 8.1 Hz, 4H). ^{13}C NMR (100 MHz, $CDCl_3$) δ (ppm) 140.67, 139.22, 131.26, 129.47, 126.13, 125.96, 123.41, 120.48, 120.28, 109.89. MS (EI-TOF, m/z): $[M]^+$ calcd for $C_{30}H_{19}BrN_2^+$: 486.07; found: 486.07.

n-BuLi in hexane (2.5 M, 4.4 mL) was added dropwise to the solution of compound 1 (9.2 mmol, 4.5 g) in THF (46 mL) at -78 ℃ under Ar. The mixture was stirring at -78 ℃ for 1 hour and the solution of dimesitylboron fluoride (10.1 mmol, 2.7 g) in THF (10 mL) was added slowly at 0 ℃. After stirring at room temperature overnight, the solution was poured into saturated NH_4Cl solution and extracted with CH_2Cl_2 by three times. The combined organic layer was washed with water and dried over Na_2SO_4. The solvent was removed under reduced pressure and the crude product was purified by silica gel column chromatography using *n*-hexane/CH_2Cl_2 (6:1, *v*/*v*) as eluent and *o*B-2Cz was obtained as pale green powder. Yield: 15% (1.4 mmol, 0.9 g). ^{1}H NMR (400 MHz, DMSO-d_6) δ (ppm) 8.10 (t, J = 7.8 Hz, 1H), 7.93 (d, J = 7.7 Hz, 2H), 7.75 (dd, J = 18.9, 7.8 Hz, 4H), 7.32 – 7.25 (m, 4H), 7.21 (d, J = 8.1 Hz, 2H), 7.15 (dt, J = 7.4, 3.3 Hz, 4H), 7.09 (t, J = 7.4 Hz, 2H), 5.69 (d, J = 7.7 Hz, 4H), 2.21 (s, 6H), 1.75 (s, 6H), 0.65 (s, 6H). ^{13}C NMR (100 MHz, $CDCl_3$) δ (ppm) 144.78, 142.97, 142.72, 139.20, 138.56, 137.42, 133.65, 132.87, 128.10, 126.49, 124.69, 124.62, 123.87, 123.13, 119.75, 119.46, 119.20, 119.06, 111.26, 111.08, 26.91, 21.22, 20.80. MS (MALDI-TOF, m/z): $[M]^+$ calcd for $C_{48}H_{41}BN_2^+$: 656.34; found: 656.35.

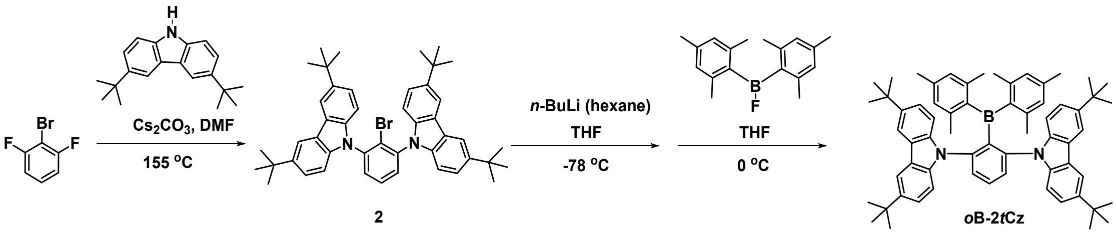

Scheme S2 Synthetic route of *o*B-2*t*Cz.

Synthesis of *o*B-2*t*Cz

Under Ar atmosphere, 3,6-di-tert-butylcarbazole (60.5 mmol, 16.9 g), Cs_2CO_3 (163.4 mmol, 53.3 g) were mixed in anhydrous DMF (160 mL). After stirring at room temperature for 1 hour, 2-bromo-1,3-difluorobenzene (27.5 mmol, 5.3 g) was added and then refluxed overnight. After cooling to room temperature, the mixture was poured into water and extracted with CH_2Cl_2 by three times. The combined organic layer was washed with water and dried over Na_2SO_4. The solvent was removed under reduced pressure and the crude product was purified by silica gel column chromatography using *n*-hexane/CH_2Cl_2 (6:1, *v*/*v*) as eluent and compound 2 was obtained as white powder. Yield: 73% (20 mmol, 12 g). ^{1}H NMR (400 MHz, $CDCl_3$) δ (ppm) 8.27 (d, J = 1.8 Hz, 4H), 7.74 – 7.70 (m, 1H), 7.69 (d, J = 5.2 Hz, 2H), 7.61 (d, J = 1.9 Hz, 2H), 7.59 (d, J = 1.9 Hz, 2H), 7.22 (d, J = 8.6 Hz, 4H), 1.57 (s, 36H). ^{13}C NMR (100 MHz, $CDCl_3$) δ (ppm) 143.05, 139.60, 139.22, 130.83, 129.23, 123.77, 123.33, 116.43, 109.36, 34.76, 32.02. MS (EI-TOF, m/z): $[M]^+$ calcd for $C_{46}H_{15}BrN_2^+$: 711.83; found: 711.33.

n-BuLi in hexane (2.5 M, 8.4 mL) was added dropwise to the solution of compound 2 (17.5 mmol, 10.5 g) in THF (140 mL) at -78 °C under Ar. The mixture was stirring at -78 °C for 1 hour and the solution of dimesitylboron fluoride (19.3 mmol, 5.2 g) in THF (20 mL) was added slowly at 0 °C. After stirring at room temperature overnight, the solution was poured into saturated NH_4Cl solution and extracted with CH_2Cl_2 by three times. The combined organic layer was washed with water and dried over Na_2SO_4. The solvent was removed under reduced pressure and the crude product was purified by silica gel column chromatography using *n*-hexane/CH_2Cl_2 (6:1, *v*/*v*) as eluent and *o*B-2*t*Cz was obtained as yellow powder. Yield: 10% (2.8 mmol, 2.5 g). ^{1}H NMR (400 MHz, $CDCl_3$) δ (ppm) 7.85 (t, J = 7.8 Hz, 1H), 7.80 (d, J = 1.9 Hz, 2H), 7.69 (d, J = 1.9 Hz, 2H), 7.60 (d, J =

7.8 Hz, 2H), 7.35 (d, $J = 1.9$ Hz, 1H), 7.33 (d, $J = 2.0$ Hz, 1H), 7.27 (d, $J = 1.9$ Hz, 1H), 7.25 (d, $J = 2.0$ Hz, 1H), 7.15 (d, $J = 8.6$ Hz, 2H), 7.07 (d, $J = 8.6$ Hz, 2H), 5.70 (d, $J = 23.0$ Hz, 4H), 2.23 (s, 6H), 1.81 (s, 6H), 1.47 (s, 18H), 1.40 (s, 18H), 0.75 (s, 6H). ^{13}C NMR (100 MHz, $CDCl_3$) δ (ppm) 145.27, 142.40, 141.82, 141.59, 141.21, 139.68, 138.70, 137.03, 133.54, 132.43, 128.02, 126.08, 123.70, 122.90, 122.31, 122.15, 115.55, 114.82, 110.74, 110.26, 34.73, 32.31, 32.24, 26.84, 21.57, 21.09. MS (MALDI-TOF, m/z): $[M]^+$ calcd for $C_{64}H_{73}BN_2^+$: 880.59; found: 880.70.

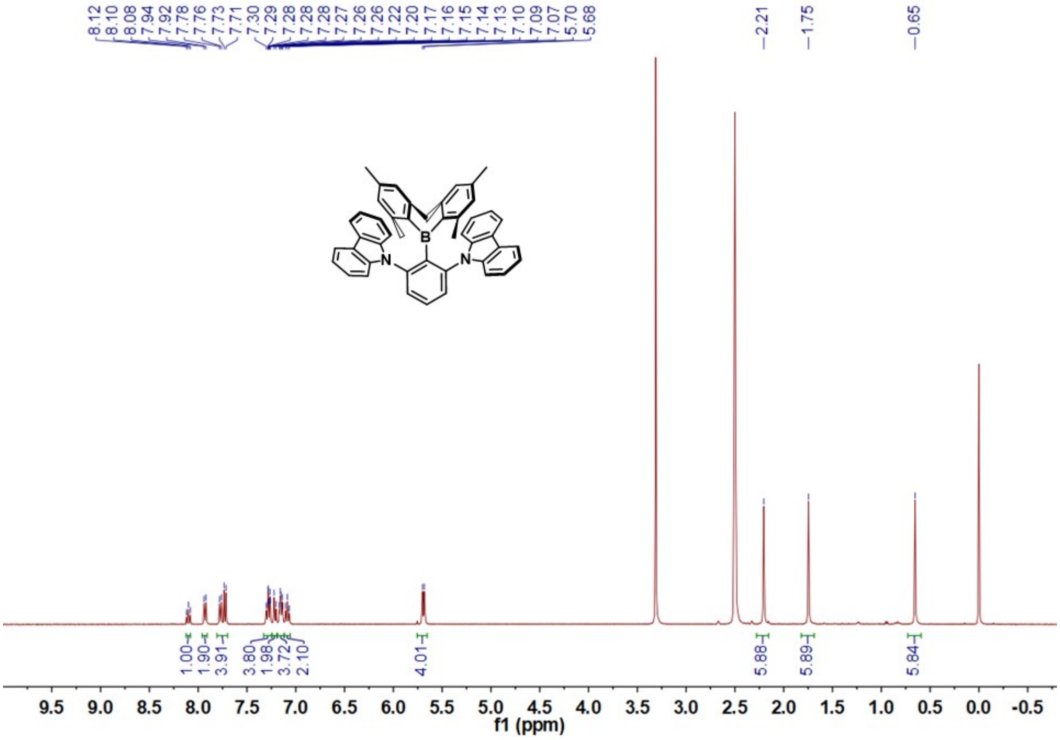

Fig. S1 ^{1}H NMR spectrum of *o*B-2Cz.

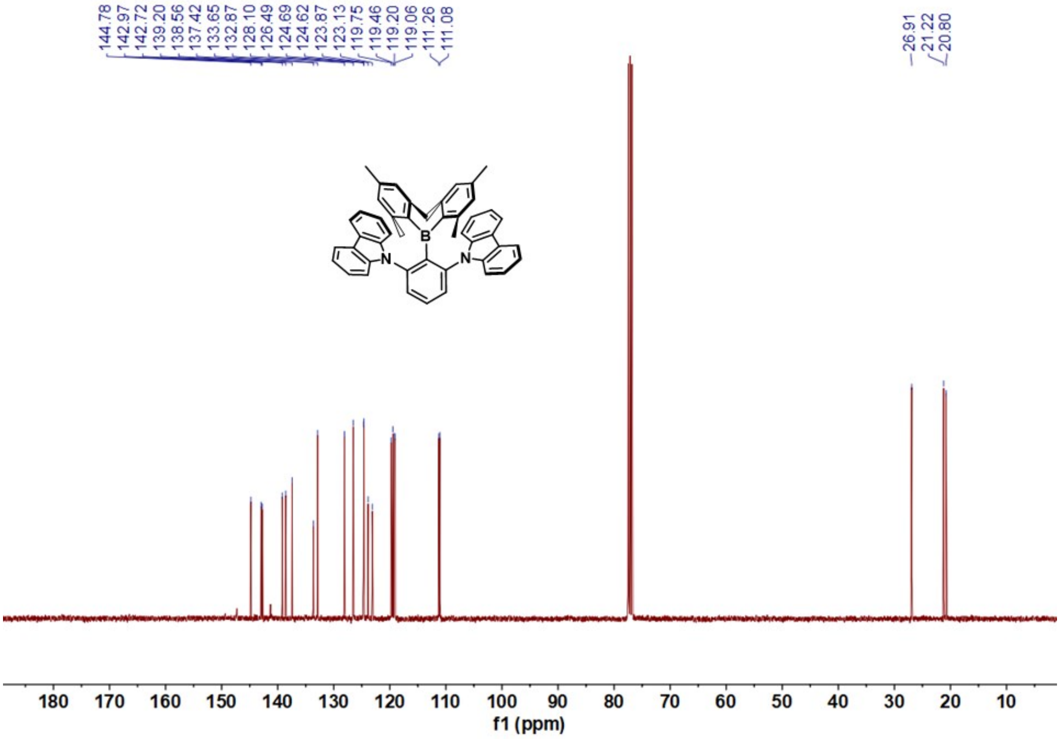

Fig. S2 ^{13}C NMR spectrum of *o*B-2Cz.

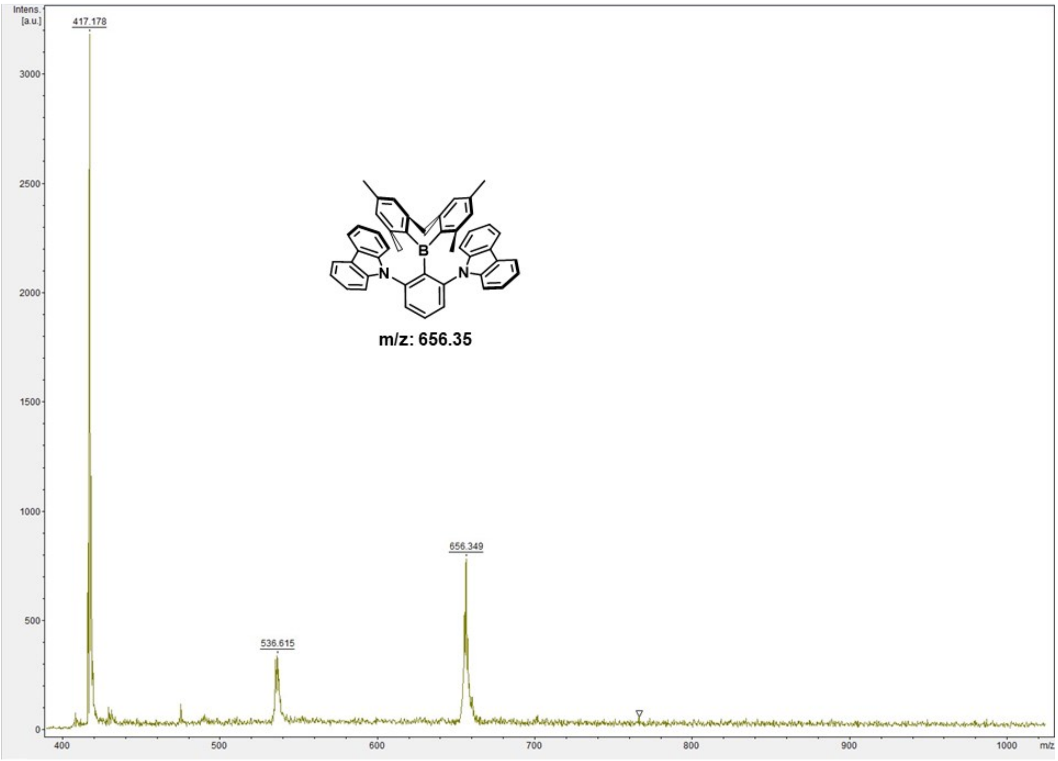

Fig. S3 MALDI-TOF mass spectrum of *o*B-2Cz.

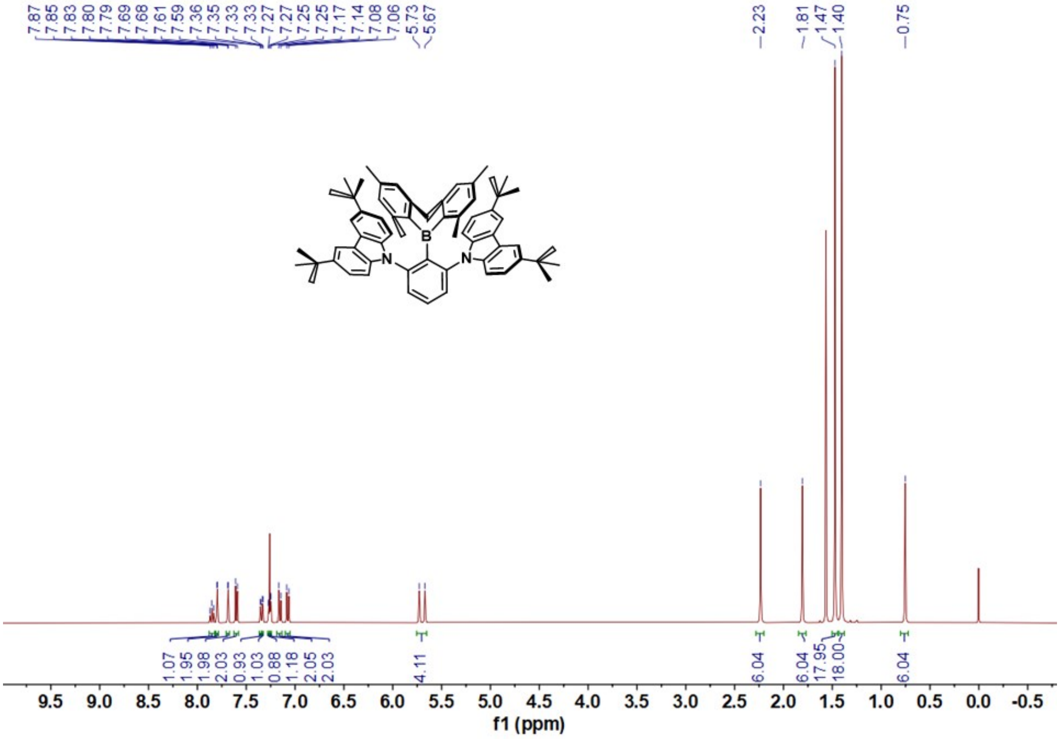

Fig. S4 ^{1}H NMR spectrum of *o*B-2*t*Cz.

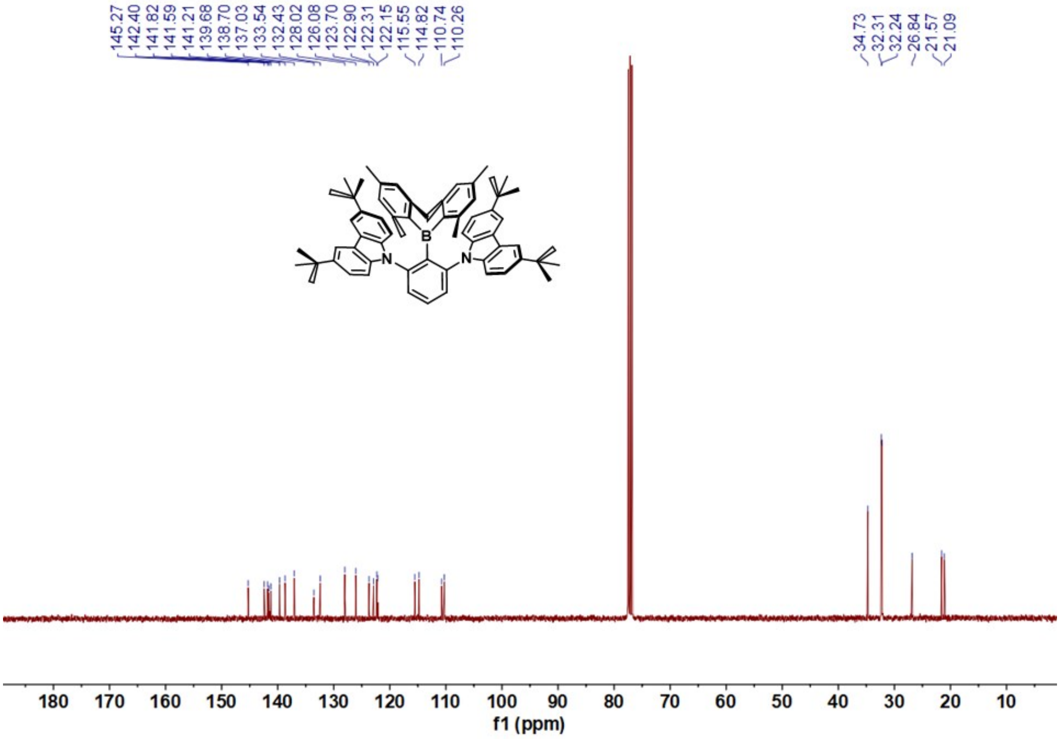

Fig. S5 ^{13}C NMR spectrum of *o*B-2*t*Cz.

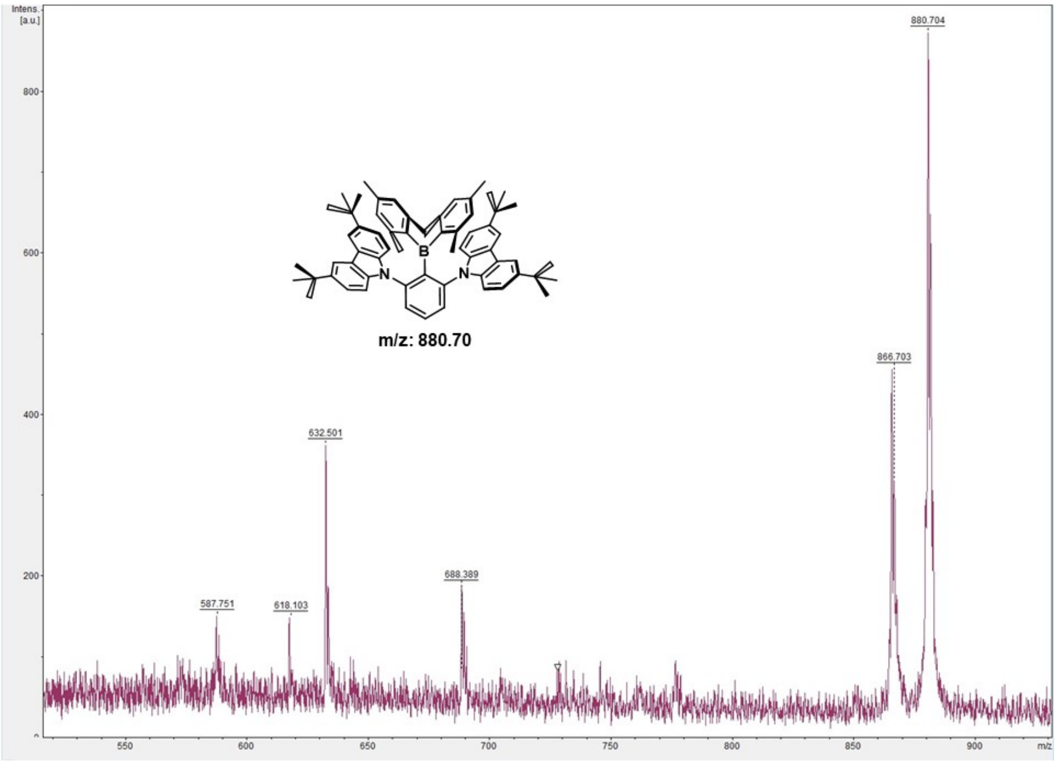

Fig. S6 MALDI-TOF mass spectrum of *o*B-2*t*Cz.

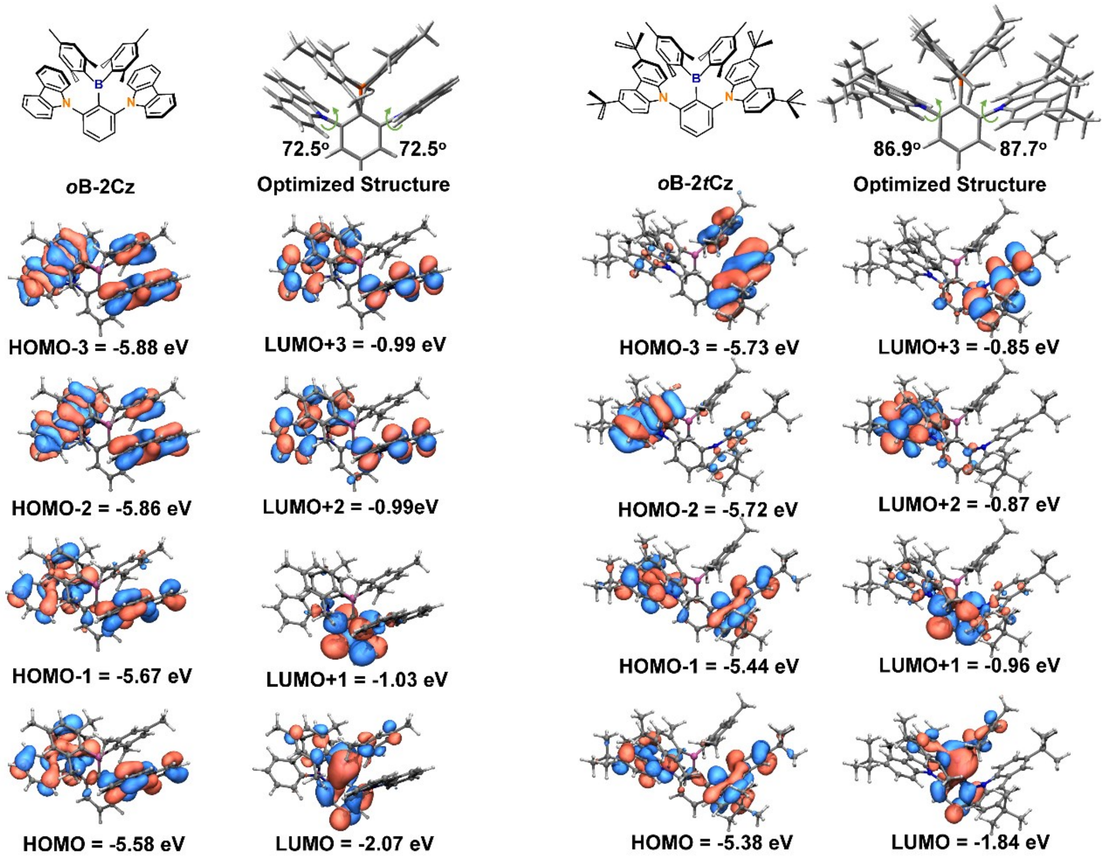

Fig. S7 The molecular structures, optimized structures, HOMO-3/LUMO+3/HOMO-2/LUMO+2/HOMO-1/LUMO+1/HOMO/LUMO distributions and the corresponding energy levels of *o*B-2Cz and *o*B-2*t*Cz.

Table S1 The hole-electron analysis of *o*B-2Cz and *o*B-2*t*Cz. D_idx is the hole-electron centroid distance. Sr is the hole-electron overlap integral. t_idx is the CT character. orb is electron configuration.

Compound	S_n/T_n	eV-S	nm-S	f-S	D_idx-S	S_r-S	t_idx-S	orb-S	eV-T	D_idx-T	S_r-T	t_idx-T	orb-T
*o*B-2Cz	1	2.9538	419.74	0.0046	0.095	0.28301	-1.480	H-L:0.985	2.7887	1.004	0.50642	-0.825	H-L:0.384; H5-L:0.329
	2	3.0503	406.47	0.0002	0.216	0.36806	-1.543	H1-L:0.954; H4-L:0.033	2.8056	1.143	0.53031	-0.554	H4-L:0.531; H1-L:0.238
	3	3.291	376.74	0.0351	1.628	0.40779	-0.080	H2-L:0.5; H4-L:0.465	2.9294	0.473	0.45125	-1.195	H-L:0.426; H5-L:0.147
	4	3.3239	373.01	0.0044	1.322	0.36213	-0.397	H3-L:0.933; H6-L:0.058	2.9885	0.097	0.71652	-1.146	H2-L2:0.214; H3-L3:0.207
	5	3.3501	370.09	0.049	1.296	0.40404	-0.487	H4-L:0.48; H2-L:0.464	3.0208	0.011	0.68566	-1.268	H2-L3:0.212; H3-L2:0.203
*o*B-2*t*Cz	1	3.0042	412.7	0.0005	0.846	0.26169	-1.202	H-L:0.986	2.8501	0.786	0.35035	-1.309	H-L:0.539; H5-L:0.097
	2	3.0881	401.5	0.0069	0.898	0.24623	-1.190	H1-L:0.985	2.9017	0.863	0.51421	-0.872	H4-L:0.244; H2-L:0.174
	3	3.3628	368.7	0.0398	0.980	0.40293	-1.076	H2-L:0.711; H4-L:0.128	2.985	0.389	0.61055	-1.669	H2-L2:0.416; H4-L2:0.062
	4	3.4417	360.24	0.0067	0.942	0.34252	-1.428	H3-L:0.83; H2-L:0.115	2.9951	0.449	0.67493	-1.760	H3-L3:0.423; H5-L3:0.056
	5	3.6553	339.19	0.0184	1.489	0.36368	-0.547	H4-L:0.755; H2-L:0.144	3.019	0.325	0.38698	-1.823	H-L:0.316; H3-L:0.127

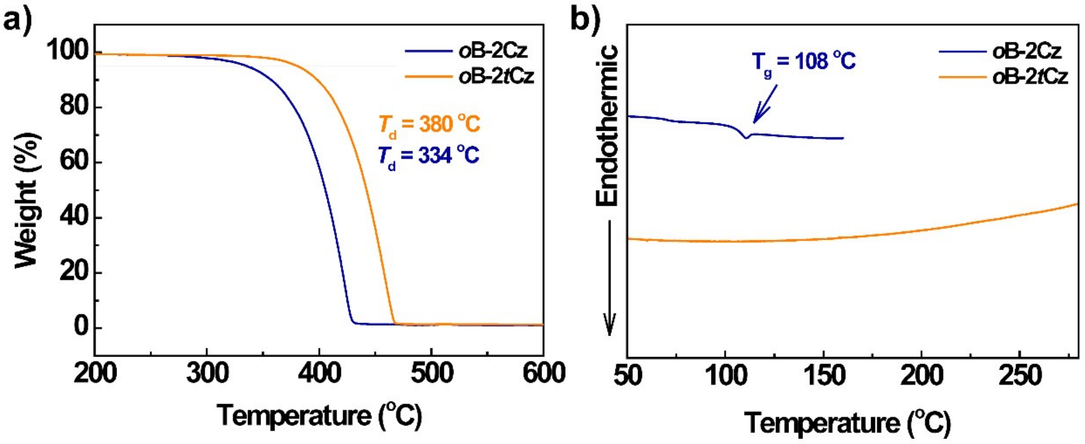

Fig. S8 a) TGA and b) DSC spectra of *o*B-2Cz and *o*B-2*t*Cz.

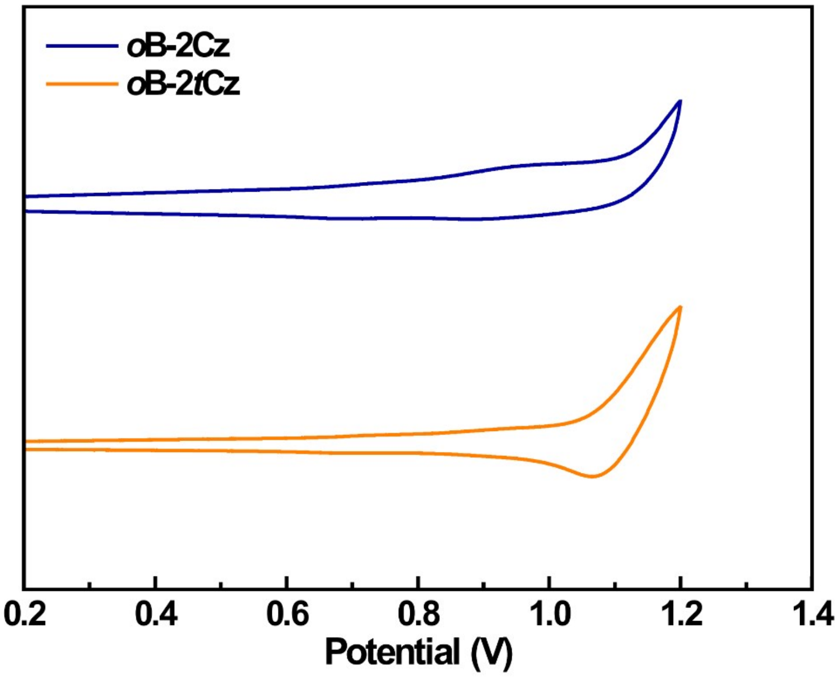

Fig. S9 Cyclic voltammogram of *o*B-2Cz and *o*B-2*t*Cz.

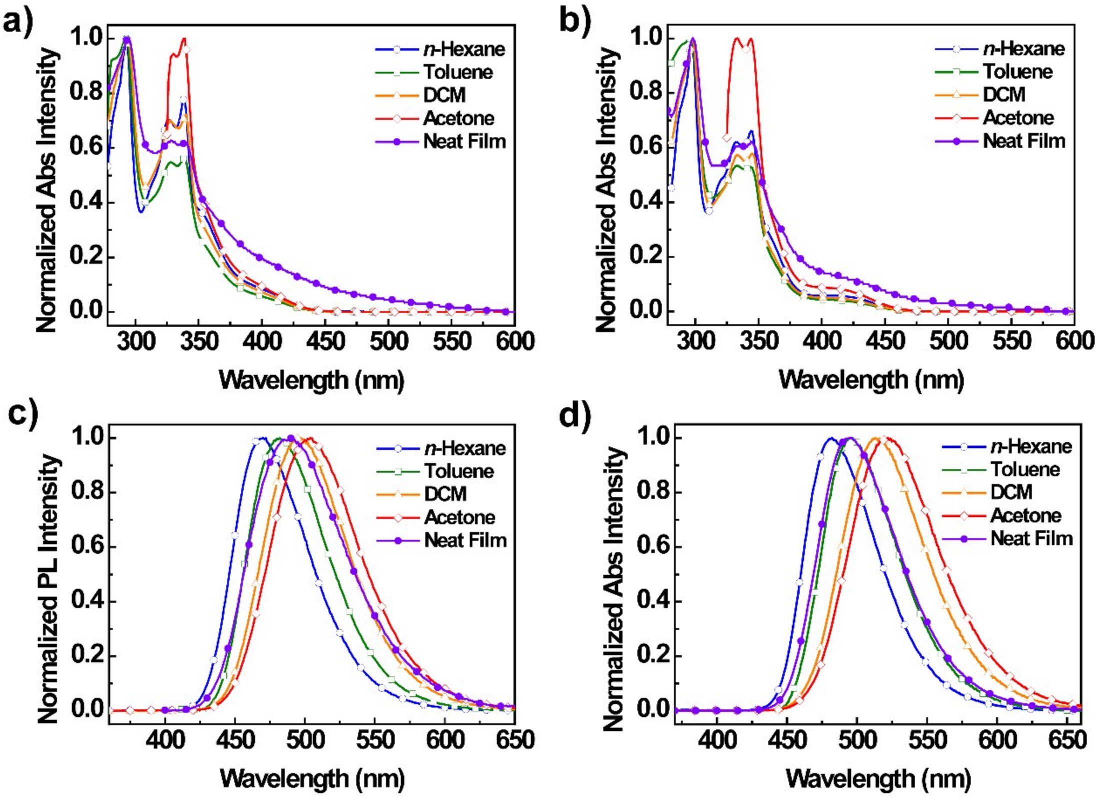

Fig. S10 UV/Vis absorption spectra of a) *o*B-2Cz and b) *o*B-2*t*Cz and photoluminescence spectra of c) *o*B-2Cz and d) *o*B-2*t*Cz performed in various solutions (10^{-5}M) and neat film at room temperature.

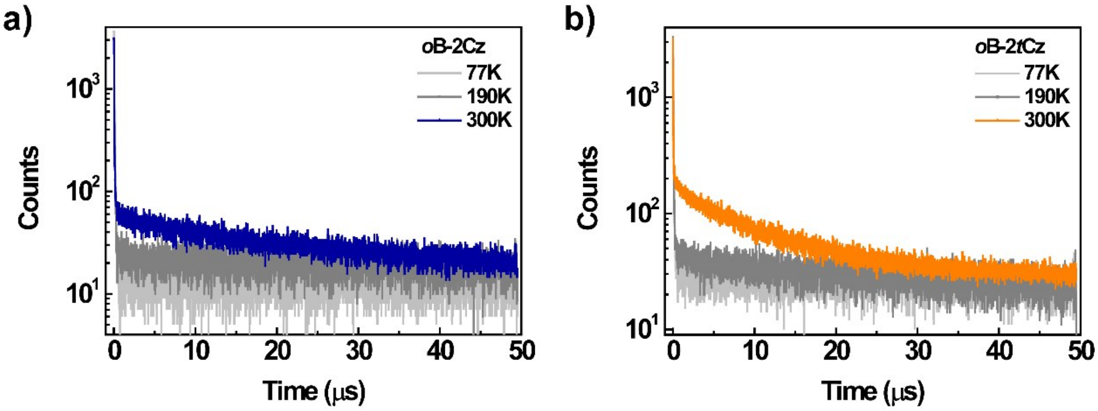

Fig. S11 The transient photoluminescence decay spectra of 10 wt.% a) *o*B-2Cz and b) *o*B-2*t*Cz doped in DPEPO film at various temperatures in degassed condition.

Calculation of Rate Constants

Intersystem crossing rate constant (k_{ISC}), reverse intersystem crossing rate constant (k_{RISC}), fluorescent decay rate constant (k_{F}) were calculated by the equations below.[4]

$$k_{\mathrm{ISC}} = \frac{\Phi_{\mathrm{d}}}{\Phi_{\mathrm{p}} + \Phi_{\mathrm{d}}} k_{\mathrm{p}} \qquad \text{equation S1}$$

$$k_{\mathrm{RISC}} = \frac{k_{\mathrm{d}} k_{\mathrm{p}} \Phi_{\mathrm{d}}}{k_{\mathrm{ISC}} \Phi_{\mathrm{p}}} \qquad \text{equation S2}$$

$$k_F = \Phi_{\mathrm{p}} k_{\mathrm{p}} \qquad \text{equation S3}$$

Table S2 Rate constants of *o*B-2Cz and *o*B-2*t*Cz.

Compound	τ_{p}[a)] (ns)	τ_{d}[a)] (μs)	Φ_{p} (%)	Φ_{d} (%)	k_{p} (10^6 s^{-1})	k_{d} (10^4 s^{-1})	k_{ISC} (10^6 s^{-1})	k_{RISC} (10^5 s^{-1})	k_{F} (10^4 s^{-1})
*o*B-2Cz	57.95	18.09	8.4	84.5	1.45	4.67	1.32	5.17	12.18
*o*B-2*t*Cz	49.78	9.69	5.3	91.0	1.06	9.39	1.01	17.06	5.64

[a)] Measured in doped film with emitters (10 wt.%) in DPEPO host.

The exciton utilization efficiency (EUE, η_{r}) was calculated by the following equation:

$$\mathrm{EQE} = \gamma \eta_{\mathrm{r}} \Phi_{PL} \eta_{\mathrm{out}} \qquad \text{equation S4}$$

where γ was the charge balance factor which was equal to 100% for a proper device; η_{out} was the light out-coupling efficiency (η_{out} = 30%).

Table S3 Comparison of device performances between this work and previous research.[1-3, 5, 6]

Emitter (wt. %)	Host	Device Performance			CIE	FWHM (nm)	k_{RISC} (10^5 s^{-1})	Reference
		CE$_{\text{max}}$ (cd/A)	PE$_{\text{max}}$ (lm/W)	EQE$_{\text{max}}$ (%)				
*o*B-2Cz (10)	DPEPO	63.3	60.4	28.1	(0.18, 0.37)	77	5.17	this work
*o*B-2*t*Cz (10)	DPEPO	84.0	71.1	27.5	(0.22, 0.49)	82	17.06	
B-oCz (non-doped)	\	11.6	7.6	8.0	(0.15, 0.17)	60	\	1
B-oTC (non-doped)	\	37.3	27.6	19.1	(0.15,0.26)	56	\	
Cz*o*B (20)	DPEPO	33.8	\	24.1	(0.139, 0.198)	\	\	2
BuCz*o*B (10)	DPEPO	56.9	\	26.1	(0.142, 0.344)	\	\	3
BuCzMe*o*B (20)	DPEPO	56.8	\	32.8	(0.135, 0.266)	\	\	
CzMe*o*B (20)	DPEPO	20.4	\	18.4	(0.138, 0.140)	\	\	
CzOMe*o*B (20)	DPEPO	13.1	\	17.3	(0.150, 0.086)	\	\	
CzBM-1 (6)	DPEPO	1.4	1.1	1.8	(0.16, 0.11)	\	0.686	5
CzBM-2 (6)	DPEPO	19.8	17.3	12.5	(0.18, 0.24)	\	2.02	
CzBM-3 (6)	DPEPO	19.3	16.8	11.7	(0.17, 0.22)	\	1.18	
CzPBM-2 (6)	DPEPO	13.8	9.6	9.5	(0.19, 0.27)	\	0.552	
CzPBM-3 (6)	DPEPO	9.4	6.5	13.3	(0.18, 0.19)	\	0.968	
CzCF3*o*B (20)	TCTA:B3PYMPM	80.2	80.7	22.9	(0.242, 0.570)	\	2.22	6
CzTF7*o*B (20)	TCTA:B3PYMPM	74.4	77.8	19.9	(0.291, 0.595)	\	1.61	
BuCzCF3*o*B (20)	TCTA:B3PYMPM	97.1	123.9	29.9	(0.330, 0.598)	\	3.24	
BuCzTF7*o*B (20)	TCTA:B3PYMPM	107.2	94.7	21.9	(0.378, 0.587)	\	2.89	

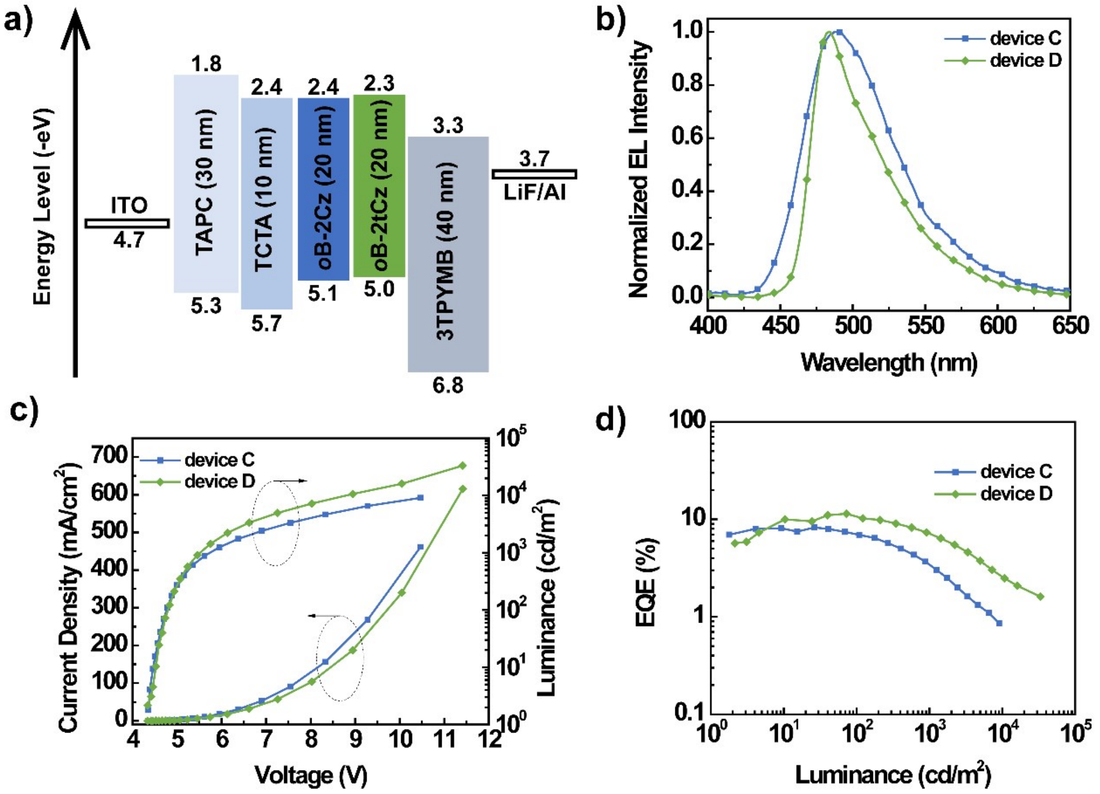

Fig. S12 a) The non-doped device structures of *o*B-2Cz and *o*B-2*t*Cz and the corresponding energy level diagrams, b) electroluminescence (EL) spectra, c) current density-voltage-luminance (*J*-*V*-*L*) characteristics, and d) EQE-luminance curves.

Table S4 Electroluminescent parameters of device C and D.

device	$V_{on}$$^{a)}$ (V)	$\lambda_{EL}$$^{b)}$ (nm)	CIE$^{b)}$ (x,y)	CE$^{c)}$ (cd/A)	PE $^{c)}$ (lm/W)	EQE$^{c)}$ (%)
C	4.3	488	(0.19, 0.39)	20.4, 8.0	14.3, 3.9	8.1, 3.6
D	4.3	483	(0.17, 0.43)	29.4, 9.5	20.2, 9.5	11.4, 6.9

$^{a)}$ Measured at luminance of 1 cd/m^2. $^{b)}$ Recorded at luminance of 1000 cd/m^2. $^{c)}$ Device performances measured at maximum and the luminance of 1000 cd/m^2, respectively.

References

1 X.-L. Chen, J.-H. Jia, R. Yu, J.-Z. Liao, M.-X. Yang and C.-Z. Lu, *Angew. Chem. Int. Ed.*, 2017, **56**, 15006-15009.

2 Y. H. Lee, S. Park, J. Oh, J. W. Shin, J. Jung, S. Yoo and M. H. Lee, *ACS Appl. Mater. Interfaces*, 2017, **9**, 24035-24042.

3 Y. H. Lee, S. Park, J. Oh, S.-J. Woo, A. Kumar, J.-J. Kim, J. Jung, S. Yoo and M. H. Lee, *Adv. Opt. Mater.*, 2018, **6**, 1800385.

4 K. Masui, H. Nakanotani and C. Adachi, *Org. Electron.*, 2013, **14**, 2721-2726.

5 P. Ganesan, D.-G. Chen, W.-C. Chen, P. Gnanasekaran, J.-A. Lin, C.-Y. Huang, M.-C. Chen, C.-S. Lee, P.-T. Chou and Y. Chi, *J. Mater. Chem. C*, 2020, **8**, 4780-4788.

6 A. Kumar, W. Lee, T. Lee, J. Jung, S. Yoo and M. H. Lee, *J. Mater. Chem. C*, 2020, **8**, 4253-4263.